The coupling of local discontinuous Galerkin and conforming finite element methods

Ilaria Perugia* Dominik Schötzau†

October 18, 2000

Abstract

The finite element formulation resulting from coupling the local discontinuous Galerkin method with a standard conforming finite element method for elliptic problems is analyzed. The transmission conditions across the interface separating the subdomains where the different formulations are applied are taken into account by a suitable definition of the so–called numerical fluxes, and the resulting coupled method is shown to be stable. Optimal a priori error estimates are derived for arbitrary meshes with possible hanging nodes and elements of various shapes. Numerical experiments validating the theoretical results are also presented.

1 Introduction

In this paper we study the finite element formulation resulting from coupling the local discontinuous Galerkin (LDG) method with a standard conforming finite element method. This coupled method, introduced in [3] in the framework of rotating electrical machines, combines the ease with which the LDG method handles hanging nodes with the lower computational cost of standard finite elements. In the above mentioned application, the fixed and the rotating parts of the domain are triangulated independently, inducing hanging nodes along the circular common boundary of the two meshes. This motivated the

*Department of Mathematics, University of Pavia, Via Ferrata 1, 27100, Pavia, Italy. E-mail: perugia@dimat.unipv.it. Supported in part by the National Science Foundation (Grant DMS-9807491) and by the Supercomputing Institute of the University of Minnesota. This work was carried out when the author was a Visiting Professor at the School of Mathematics, University of Minnesota.

†School of Mathematics, University of Minnesota, Minneapolis, MN 55455, USA. E-mail: schoetza@math.umn.edu.

use of the LDG method in a small neighborhood of the common boundary and the use of a standard conforming finite element method elsewhere. Preliminary numerical results presented in [3] show that the resulting method is very promising; this is why we carry out its a priori error analysis in this paper. The coupling of LDG and standard conforming finite element methods might also be suited for dealing with multi–physics or multi–material problems, where different physical models (and, thus, different numerical methods) are applied in different parts of the computational domain. Indeed, discontinuous Galerkin (DG) methods, in general, proved to be very efficient to handle convection terms, due to their structure inherited from the corresponding discretizations of non–linear conservation laws. Furthermore, they can easily handle elements of various shapes and local spaces of different type and, hence, are ideally suited for hp–adaptivity. For recent surveys on DG methods, see [16, 19].

There exists a large body of literature dealing with the coupling of methods applied in different subdomains, particularly in the case of non–matching grids. A natural idea is to enforce continuity across interfaces by Lagrange multiplier techniques, giving rise to the so–called mortar method and its variants; see, e.g., [1, 8, 9, 10, 23] and the references therein. We also mention [2, 4, 13, 26], where particular attention is paid to the handling of non–matching grids arising in practical applications. A related approach has also been adopted in [27] to impose transmission conditions in the coupling of mixed and conforming finite elements. In mortar methods, the Lagrange multipliers are introduced as new unknowns and have to be solved for. Thus, to obtain stable discretizations, either an inf–sup condition must be satisfied, or special stabilization techniques must be applied; see, e.g., [5, 6, 12, 24] and the references therein.

The alternative approach followed in this paper is to enforce interface conditions with DG techniques. The main feature of DG methods is that they do not require continuity across element boundaries. This is also a key property of the mortar finite element method. However, in DG methods there are no Lagrange multipliers associated with the continuity constraints; instead, the Lagrange multipliers are replaced by the so–called numerical fluxes, which are fixed functions of the unknowns. This makes simple not only the handling of non–matching grids, but also the coupling with other formulations. The application of DG methods in certain subdomains can therefore be easily implemented within existing conforming finite element codes. In the context of domain decomposition with non–matching grids, DG approaches have recently been analyzed in [7, 25]. There, the continuity constraints are imposed in a discontinuous way by Nitsche's method, originally designed to weakly enforced Dirichlet boundary conditions (see also [24]). The DG method adopted here is the LDG method introduced in [20] for transient convection-diffusion problems, and analyzed in [14] for purely elliptic problems; see also [17] for the special case of Cartesian grids.

The model problem we consider is the Poisson equation with Dirichlet and Neumann boundary conditions, namely,

$$\begin{aligned} -\Delta u &= f && \text{in } \Omega, \\ u &= g_{\mathcal{D}} && \text{on } \Gamma_{\mathcal{D}}, \\ \nabla u \cdot \boldsymbol{n} &= \boldsymbol{g}_{\mathcal{N}} \cdot \boldsymbol{n} && \text{on } \Gamma_{\mathcal{N}}, \end{aligned} \tag{1}$$

where Ω is a bounded domain of $\mathbb{R}^d$, $d = 2, 3$, and $\boldsymbol{n}$ is the outward unit normal to its boundary $\partial\Omega = \overline{\Gamma}_{\mathcal{D}} \cup \overline{\Gamma}_{\mathcal{N}}$. We assume that the $(d-1)$–dimensional measure of $\Gamma_{\mathcal{D}}$ is non–zero.

Consider now a partition of Ω into two disjoint subdomains Ω_1 and Ω_2 with interface $\Gamma := \partial\Omega_1 \cap \partial\Omega_2$. We discretize problem (1) by using the LDG method in Ω_1, and a standard continuous method in Ω_2. To do that, we set $u^i := u|_{\Omega_i}$, $\Gamma^i_{\mathcal{D}} = \Gamma_{\mathcal{D}} \cap \partial\Omega_i$, $\Gamma^i_{\mathcal{N}} = \Gamma_{\mathcal{N}} \cap \partial\Omega_i$, and denote by $\boldsymbol{n}_i$ the outward unit normal vector to $\partial\Omega_i \cap \Gamma$, $i = 1, 2$. The LDG method in Ω_1 is obtained by using a discretization that was originally applied to first–order hyperbolic problems. Hence, we introduce the auxiliary variable $\boldsymbol{q} = \nabla u^1$ on Ω_1 and rewrite problem (1) as the following equivalent transmission problem:

$$\boldsymbol{q} = \nabla u^1 \qquad \text{in } \Omega_1, \tag{2}$$

$$-\nabla \cdot \boldsymbol{q} = f \qquad \text{in } \Omega_1, \tag{3}$$

$$-\Delta u^2 = f \qquad \text{in } \Omega_2, \tag{4}$$

$$u^1 = u^2 \qquad \text{on } \Gamma, \tag{5}$$

$$\boldsymbol{q} \cdot \boldsymbol{n}_1 = -\nabla u^2 \cdot \boldsymbol{n}_2 \qquad \text{on } \Gamma, \tag{6}$$

with boundary conditions

$$u^1 = g_{\mathcal{D}} \qquad \text{on } \Gamma^1_{\mathcal{D}}, \tag{7}$$

$$u^2 = g_{\mathcal{D}} \qquad \text{on } \Gamma^2_{\mathcal{D}}, \tag{8}$$

$$\boldsymbol{q} \cdot \boldsymbol{n} = \boldsymbol{g}_{\mathcal{N}} \cdot \boldsymbol{n} \qquad \text{on } \Gamma^1_{\mathcal{N}}, \tag{9}$$

$$\nabla u^2 \cdot \boldsymbol{n} = \boldsymbol{g}_{\mathcal{N}} \cdot \boldsymbol{n} \qquad \text{on } \Gamma^2_{\mathcal{N}}. \tag{10}$$

In Ω_1, these equations are nothing but the first–order equations used to define classical mixed finite element methods (see [11], for instance). However in the

LDG method, the auxiliary variable $\boldsymbol{q}$ can be eliminated from the equations, which is in general not the case for classical mixed methods.

The main contribution of this paper is to show how LDG and conforming finite element methods can be coupled by a suitable definition of the numerical fluxes, giving rise to a stable method. The analysis of the resulting method can then be carried out in an almost straightforward way by using the abstract setting of [14]. We first obtain a priori error estimates for the case where polynomials of the same degree k are used to approximate all the solution components $\boldsymbol{q}$, u^1 and u^2, and then also explore the situation in which polynomials of the lower degree $k-1$ are used to approximate $\boldsymbol{q}$. This is a novelty of the analysis presented here, as compared to [14]. Mixed order LDG approximations are also investigated in [18] for the Stokes system. The obtained rates of convergence are summarized in Table 1, in dependence of a stabilization parameter in the definition of the numerical fluxes, chosen of order $\mathcal{O}(1)$ or $\mathcal{O}(1/h)$, h being the mesh–size.

Stabilization parameter	Approximation degrees for $(\boldsymbol{q}, u^1, u^2)$	L^2–error in $\boldsymbol{q}$ and ∇u^2	L^2–error in u
$\mathcal{O}(1)$	$k,\ k,\ k$	k	$k+1/2$
$\mathcal{O}(1/h)$	$k,\ k,\ k$	k	$k+1$
$\mathcal{O}(1)$	$k-1,\ k,\ k$	$k-1/2$	k
$\mathcal{O}(1/h)$	$k-1,\ k,\ k$	k	$k+1$

Table 1: Rates of convergence for smooth solutions and $k \geq 1$.

The paper is organized as follows. In Section 2, we introduce the coupled LDG/conforming finite element method and show that it defines a unique approximate solution. Then, in Section 3, we state our main result regarding convergence of the method and error estimates, and provide a detailed proof. In Section 4, we present a series of numerical results testing the sharpness of our estimates on unstructured matching as well as non–matching grids consisting of triangles. We end with some concluding remarks in Section 5.

2 Coupling LDG and continuous finite elements

In this section, the coupled finite element discretization of the transmission problem (2)–(10) is presented and existence and uniqueness of discrete solutions are proved, after recasting the problem in a standard mixed setting.

Since the Dirichlet boundary condition (8) on $\Gamma^2_{\mathcal{D}}$ has to be imposed in a standard conforming fashion, we assume, in order to simplify the presentation, that $g_{\mathcal{D}} = 0$ on $\Gamma^2_{\mathcal{D}}$. Condition (7) on $\Gamma^1_{\mathcal{D}}$ will be imposed in a discontinuous way by the numerical fluxes defined in Section 2.1.

2.1 The coupled finite element formulation

We consider triangulations $\mathcal{T}_h^1$ and $\mathcal{T}_h^2$ of Ω_1 and Ω_2, respectively, where h denotes the mesh–size defined by $h := \max_{K \in \mathcal{T}_h^1 \cup \mathcal{T}_h^1} h_K$, h_K being the diameter of the element K. For the definition of the coupled finite element method, we do not impose any restriction on the triangulations $\mathcal{T}_h^1$ and $\mathcal{T}_h^2$ at this point. They may contain elements of several shapes (for example iso–parametric elements in $\mathcal{T}_h^2$) and can be non–matching at the interface Γ. Hanging nodes can also be present in both $\mathcal{T}_h^1$ and $\mathcal{T}_h^2$. Possible hanging nodes in $\mathcal{T}_h^1$ are easily dealt with by the LDG method, whereas the handling of possible hanging nodes in $\mathcal{T}_h^2$ by means of a conforming method is not straightforward and typically involves major restrictions on the kinds of non–matching grids that are allowed (see [21], for instance).

Multiplying equations (2)–(4) by test functions and integrating by parts over the corresponding domains, it can be seen that the solution $(\boldsymbol{q}, u^1, u^2)$, u^2 with zero trace on $\Gamma^2_{\mathcal{D}}$, of problem (2)–(10) satisfies

$$\int_K \boldsymbol{q} \cdot \boldsymbol{r} \, d\boldsymbol{x} + \int_K u^1 \, \nabla \cdot \boldsymbol{r} \, d\boldsymbol{x} - \int_{\partial K} u^1 \, \boldsymbol{r} \cdot \boldsymbol{n}_K \, ds = 0, \tag{11}$$

$$\int_K \boldsymbol{q} \cdot \nabla v^1 \, d\boldsymbol{x} - \int_{\partial K} v^1 \, \boldsymbol{q} \cdot \boldsymbol{n}_K \, ds = \int_K f \, v^1 \, d\boldsymbol{x}, \tag{12}$$

for piecewise smooth functions $\boldsymbol{r}$ and v^1 and for all elements $K \in \mathcal{T}_h^1$ (we denote by $\boldsymbol{n}_K$ the outward unit normal to ∂K), and

$$\int_{\Omega_2} \nabla u^2 \cdot \nabla v^2 \, d\boldsymbol{x} - \int_\Gamma \nabla u^2 \cdot \boldsymbol{n}_2 v^2 \, ds = \int_{\Omega_2} f \, v^2 \, d\boldsymbol{x} + \int_{\Gamma^2_{\mathcal{N}}} \boldsymbol{g}_{\mathcal{N}} \cdot \boldsymbol{n} \, v^2 \, ds, \tag{13}$$

for smooth functions v^2, with $v^2|_{\Gamma^2_{\mathcal{D}}} = 0$.

Equations (11)–(12) and (13) have to be coupled through the transmission conditions (5) and (6). Condition (6) is imposed by replacing $\nabla u^2 \cdot \boldsymbol{n}_2$ by $-\boldsymbol{q} \cdot \boldsymbol{n}_1$ in equation (13), which becomes

$$\int_{\Omega_2} \nabla u^2 \cdot \nabla v^2 \, d\boldsymbol{x} + \int_\Gamma \boldsymbol{q} \cdot \boldsymbol{n}_1 v^2 \, ds = \int_{\Omega_2} f \, v^2 \, d\boldsymbol{x} + \int_{\Gamma^2_{\mathcal{N}}} \boldsymbol{g}_{\mathcal{N}} \cdot \boldsymbol{n} \, v^2 \, ds, \tag{14}$$

while condition (5) will be imposed at the discrete level by choosing the numerical fluxes in the LDG method in a suitable way.

Equations (11)–(12) and (14) are well defined for $(\boldsymbol{q}, u^1, u^2)$, $(\boldsymbol{r}, v^1, v^2)$ in $\boldsymbol{Q} \times V \times W$, where

$$\begin{aligned}
\boldsymbol{Q} &:= \{\boldsymbol{r} \in L^2(\Omega_1)^d \ : \ \boldsymbol{r}\big|_K \in H^1(K)^d, \ \forall K \in \mathcal{T}_h^1\},\\
V &:= \{v^1 \in L^2(\Omega_1) \ : \ v^1\big|_K \in H^1(K), \ \forall K \in \mathcal{T}_h^1\},\\
W &:= \{v^2 \in H^1(\Omega_2) \ : \ v^2|_{\Gamma^2_{\mathcal{D}}} = 0\}.
\end{aligned}$$

Next, we approximate the exact solution $(\boldsymbol{q}, u^1, u^2)$ in the finite element space $\boldsymbol{Q}_h \times V_h \times W_h \subset \boldsymbol{Q} \times V \times W$, where

$$\begin{aligned}
\boldsymbol{Q}_h &:= \{\boldsymbol{r} \in L^2(\Omega_1)^d \ : \ \boldsymbol{r}\big|_K \in \mathcal{R}(K)^d, \ \forall K \in \mathcal{T}_h^1\},\\
V_h &:= \{v^1 \in L^2(\Omega_1) \ : \ v^1\big|_K \in \mathcal{S}^1(K), \ \forall K \in \mathcal{T}_h^1\},\\
W_h &:= \{v^2 \in H^1(\Omega_2) \ : \ v^2|_{\Gamma^2_{\mathcal{D}}} = 0, \ v^2\big|_K \in \mathcal{S}^2(K), \ \forall K \in \mathcal{T}_h^2\}.
\end{aligned}$$

The local spaces $\mathcal{R}(K)$ and $\mathcal{S}^i(K)$, $i = 1, 2$, typically consist of polynomials or mapped polynomials. The space W_h is a standard conforming finite element space, whereas the functions in $\boldsymbol{Q}_h$ and V_h are completely discontinuous across interelement boundaries. On the LDG side, we require that the local spaces $\mathcal{R}(K)$ and $\mathcal{S}^1(K)$ satisfy the following mild inclusions

$$\nabla \mathcal{S}^1(K) \subset \mathcal{R}(K)^d, \qquad \forall K \in \mathcal{T}_h^1. \tag{15}$$

Starting from (11)–(12) and (14), and approximating the traces of u^1 and $\boldsymbol{q}$ on the boundary of the elements of $\mathcal{T}_h^1$ by the so-called *numerical fluxes*, denoted in the following by $\widehat{u}_h^1$ and $\widehat{\boldsymbol{q}}_h$, the approximate solution $(\boldsymbol{q}_h, u_h^1, u_h^2) \in \boldsymbol{Q}_h \times V_h \times W_h$ is defined by imposing

$$\int_K \boldsymbol{q}_h \cdot \boldsymbol{r} \, d\boldsymbol{x} + \int_K u_h^1 \, \nabla \cdot \boldsymbol{r} \, d\boldsymbol{x} - \int_{\partial K} \widehat{u}_h^1 \, \boldsymbol{r} \cdot \boldsymbol{n}_K \, ds = 0, \tag{16}$$

$$\int_K \boldsymbol{q}_h \cdot \nabla v^1 \, d\boldsymbol{x} - \int_{\partial K} v^1 \, \widehat{\boldsymbol{q}}_h \cdot \boldsymbol{n}_K \, ds = \int_K f \, v^1 \, d\boldsymbol{x}, \tag{17}$$

for all test functions $(\boldsymbol{r}, v^1) \in \boldsymbol{Q}_h \times V_h$ and for all $K \in \mathcal{T}_h^1$, and

$$\int_{\Omega_2} \nabla u_h^2 \cdot \nabla v^2 \, d\boldsymbol{x} + \int_\Gamma \widehat{\boldsymbol{q}}_h \cdot \boldsymbol{n}_1 v^2 \, ds = \int_{\Omega_2} f \, v^2 \, d\boldsymbol{x} + \int_{\Gamma^2_{\mathcal{N}}} \boldsymbol{g}_{\mathcal{N}} \cdot \boldsymbol{n} \, v^2 \, ds, \tag{18}$$

for all test function $v^2 \in W_h$.

Some notation needs to be introduced before defining the numerical fluxes $\widehat{u}_h^1$ and $\widehat{\boldsymbol{q}}_h$ in (16), (17) and (18). Let K^+ and K^- be two adjacent elements of $\mathcal{T}_h^1$, and let $\boldsymbol{x}$ be an arbitrary point of the set $e = \partial K^+ \cap \partial K^-$, which is assumed to have a non–zero $(d-1)$–dimensional measure. Since K^+ and K^- can be non–matching, e is not necessarily a complete face of an element in $\mathcal{T}_h^1$. Let $\boldsymbol{n}^+$ and $\boldsymbol{n}^-$ be the corresponding outward unit normals at the point $\boldsymbol{x}$. For a function $(\boldsymbol{r}, v)$ smooth inside each element $K^\pm$, denote by $(\boldsymbol{r}^\pm, v^\pm)$ the traces of $(\boldsymbol{r}, v)$ on e from the interior of $K^\pm$. Then, the mean values $\{\!\{\cdot\}\!\}$ and jumps $[\![\cdot]\!]$ at $\boldsymbol{x} \in e$ are defined as follows:

$$\begin{aligned} \{\!\{v\}\!\} &:= (v^+ + v^-)/2, & \{\!\{\boldsymbol{r}\}\!\} &:= (\boldsymbol{r}^+ + \boldsymbol{r}^-)/2, \\ [\![v]\!] &:= v^+\boldsymbol{n}^+ + v^-\boldsymbol{n}^-, & [\![\boldsymbol{r}]\!] &:= \boldsymbol{r}^+ \cdot \boldsymbol{n}^+ + \boldsymbol{r}^- \cdot \boldsymbol{n}^-. \end{aligned}$$

Note that the jump in v is a vector and the jump in $\boldsymbol{r}$ is a scalar which only involves the normal component of $\boldsymbol{r}$.

With this notation, we are now ready to define the numerical fluxes $\widehat{u}_h^1$ and $\widehat{\boldsymbol{q}}_h$ in (16), (17) and (18). For $\boldsymbol{x} \in \partial K$, $K \in \mathcal{T}_h^1$, we set:

$$\widehat{u}_h^1(\boldsymbol{x}) = \begin{cases} \{\!\{u_h^1\}\!\} + \boldsymbol{\beta} \cdot [\![u_h^1]\!] & \text{if } \boldsymbol{x} \in \partial K \setminus \partial\Omega_1, \\ g_{\mathcal{D}} & \text{if } \boldsymbol{x} \in \partial K \cap \Gamma_{\mathcal{D}}^1, \\ u_h^1 & \text{if } \boldsymbol{x} \in \partial K \cap \Gamma_{\mathcal{N}}^1, \\ u_h^2 & \text{if } \boldsymbol{x} \in \partial K \cap \Gamma, \end{cases} \tag{19}$$

and

$$\widehat{\boldsymbol{q}}_h(\boldsymbol{x}) = \begin{cases} \{\!\{\boldsymbol{q}_h\}\!\} - \alpha[\![u_h^1]\!] - \boldsymbol{\beta}[\![\boldsymbol{q}_h]\!] & \text{if } \boldsymbol{x} \in \partial K \setminus \partial\Omega_1, \\ \boldsymbol{q}_h - \alpha(u_h^1 - g_{\mathcal{D}})\boldsymbol{n} & \text{if } \boldsymbol{x} \in \partial K \cap \Gamma_{\mathcal{D}}^1, \\ \boldsymbol{g}_{\mathcal{N}} & \text{if } \boldsymbol{x} \in \partial K \cap \Gamma_{\mathcal{N}}^1, \\ \boldsymbol{q}_h - \alpha(u_h^1 - u_h^2)\boldsymbol{n}_1 & \text{if } \boldsymbol{x} \in \partial K \cap \Gamma. \end{cases} \tag{20}$$

Here, the scalar $\alpha = \alpha(\boldsymbol{x})$ and the vector $\boldsymbol{\beta} = \boldsymbol{\beta}(\boldsymbol{x})$ are auxiliary parameters. Their purpose is to enhance the stability and accuracy properties of the LDG method (see [20] and [14]). Notice that the fluxes defined by (19) and (20) are consistent in the sense that equations (16), (17) and (18) coincide with (11), (12) and (14) for the exact solution $(\boldsymbol{q}, u^1, u^2)$. We also remark that the numerical fluxes are chosen in such a way that they impose the transmission condition (5) over Γ. Indeed, the edges that lie on the interface Γ are considered as "Dirichlet" edges from the LDG side, with Dirichlet datum u_h^2. Furthermore, since $\widehat{u}_h^1$ does not depend on $\boldsymbol{q}_h$, the unknown $\boldsymbol{q}_h$ can be computed element by element in terms of u_h^1 by using equation (16), and then substituted into equation (17) (see [20] for more details), giving rise to a problem in the unknowns u_h^1 and u_h^2 only. This local solvability gives the name to the LDG method.

2.2 The mixed setting

The study of the coupled finite element method is greatly facilitated if we recast its formulation in a mixed setting. To do that, we sum (16) and (17) over all elements $K \in \mathcal{T}_h^1$, take into account (19) and (20), and obtain the following equivalent formulation of problem (16)–(18): Find $(\boldsymbol{q}_h, u_h^1, u_h^2) \in \boldsymbol{Q}_h \times V_h \times W_h$ such that

$$a(\boldsymbol{q}_h, \boldsymbol{r}) \ + b(u_h^1, \boldsymbol{r}) + s(\boldsymbol{r}, u_h^2) \ = F(\boldsymbol{r}), \tag{21}$$

$$b(v^1, \boldsymbol{q}_h) - c(u_h^1, v^1) + t(v^1, u_h^2) \ = G(v^1), \tag{22}$$

$$s(\boldsymbol{q}_h, v^2) + t(u_h^1, v^2) - m(u_h^2, v^2) = H(v^2), \tag{23}$$

for all test functions $(\boldsymbol{r}, v^1, v^2) \in \boldsymbol{Q}_h \times V_h \times W_h$. Here, the bilinear forms a, b, c, m, s and t are given by

$$\begin{aligned}
a(\boldsymbol{q}, \boldsymbol{r}) &= \int_{\Omega_1} \boldsymbol{q} \cdot \boldsymbol{r} \, d\boldsymbol{x}, \\
b(u^1, \boldsymbol{r}) &= \sum_{K \in \mathcal{T}_h^1} \int_K u^1 \nabla \cdot \boldsymbol{r} \, d\boldsymbol{x} - \int_{\mathcal{E}_\mathcal{I}} (\{\!\{u^1\}\!\} + \boldsymbol{\beta} \cdot [\![u^1]\!]) [\![\boldsymbol{r}]\!] \, ds \\
&\quad - \int_{\Gamma_\mathcal{N}^1} u^1 \boldsymbol{r} \cdot \boldsymbol{n} \, ds, \\
c(u^1, v^1) &= \int_{\mathcal{E}_\mathcal{I}} \alpha [\![u^1]\!] \cdot [\![v^1]\!] \, ds + \int_{\Gamma_\mathcal{D}^1} \alpha u^1 v^1 \, ds + \int_\Gamma \alpha u^1 v^1 \, ds, \\
m(u^2, v^2) &= \int_{\Omega_2} \nabla u^2 \cdot \nabla v^2 \, d\boldsymbol{x} + \int_\Gamma \alpha u^2 v^2 \, ds, \\
s(\boldsymbol{q}, v^2) &= -\int_\Gamma \boldsymbol{q} \cdot \boldsymbol{n}_1 \, v^2 \, ds, \\
t(u^1, v^2) &= \int_\Gamma \alpha u^1 v^2 \, ds,
\end{aligned}$$

where $\mathcal{E}_\mathcal{I}$ denotes the union of all interior faces of the triangulation $\mathcal{T}_h^1$. The functionals F, G and H are defined by

$$\begin{aligned}
F(\boldsymbol{r}) &= \int_{\Gamma_\mathcal{D}^1} g_\mathcal{D} \, \boldsymbol{r} \cdot \boldsymbol{n} \, ds, \\
G(v^1) &= -\int_{\Omega_1} f \, v^1 \, d\boldsymbol{x} - \int_{\Gamma_\mathcal{D}^1} \alpha g_\mathcal{D} \, v^1 \, ds - \int_{\Gamma_\mathcal{N}^1} \boldsymbol{g}_\mathcal{N} \cdot \boldsymbol{n} \, v^1 \, ds, \\
H(v^2) &= -\int_{\Omega_2} f \, v^2 \, d\boldsymbol{x} - \int_{\Gamma_\mathcal{N}^2} \boldsymbol{g}_\mathcal{N} \cdot \boldsymbol{n} \, v^2 \, ds.
\end{aligned}$$

Notice that, integrating by parts the term $\sum_{K\in\mathcal{T}_h^1}\int_K u^1\nabla\cdot\boldsymbol{r}d\boldsymbol{x}$, the form $b(u^1,\boldsymbol{r})$ can be expressed as

$$\begin{aligned} b(u^1,\boldsymbol{r}) \quad = \quad & -\sum_{K\in\mathcal{T}_h^1}\int_K \boldsymbol{r}\cdot\nabla u^1\,d\boldsymbol{x}+\int_{\mathcal{E}_\mathcal{I}}(\{\!\{\boldsymbol{r}\}\!\}-\boldsymbol{\beta}[\![\boldsymbol{r}]\!])\cdot[\![u^1]\!]\,ds \\ & +\int_{\Gamma_\mathcal{D}^1}\boldsymbol{r}\cdot\boldsymbol{n}u^1\,ds+\int_\Gamma \boldsymbol{r}\cdot\boldsymbol{n}_1u^1\,ds. \end{aligned} \tag{24}$$

By introducing

$$\begin{aligned} \mathcal{A}(\boldsymbol{q},u^1,u^2;\boldsymbol{r},v^1,v^2) := {} & a(\boldsymbol{q},\boldsymbol{r})+b(u^1,\boldsymbol{r})+s(\boldsymbol{r},u^2)-b(v^1,\boldsymbol{q}) \\ & +c(u^1,v^1)-t(v^1,u^2)-s(\boldsymbol{q},v^2)-t(u^1,v^2)+m(u^2,v^2), \end{aligned}$$

and

$$\mathcal{F}(\boldsymbol{r},v^1,v^2):=F(\boldsymbol{r})-G(v^1)-H(v^2),$$

problem (21)–(23) can also be written in the following compact form:

Find $(\boldsymbol{q}_h,u_h^1,u_h^2)\in\boldsymbol{Q}_h\times V_h\times W_h$ such that

$$\mathcal{A}(\boldsymbol{q}_h,u_h^1,u_h^2;\boldsymbol{r},v^1,v^2)=\mathcal{F}(\boldsymbol{r},v^1,v^2) \tag{25}$$

for all $(\boldsymbol{r},v^1,v^2)\in\boldsymbol{Q}_h\times V_h\times W_h$.

The numerical fluxes have been designed in such a way that the method is stable in a problem–related seminorm.

Proposition 2.1 *For $(\boldsymbol{q},u^1,u^2)\in\boldsymbol{Q}\times V\times W$ we have*

$$\mathcal{A}(\boldsymbol{q},u^1,u^2;\boldsymbol{q},u^1,u^2)=|(\boldsymbol{q},u^1,u^2)|_\mathcal{A}^2,$$

where the seminorm $|(\boldsymbol{q},u^1,u^2)|_\mathcal{A}^2$ is defined as the quantity

$$\|\boldsymbol{q}\|_{0,\Omega_1}^2+\int_{\mathcal{E}_\mathcal{I}}\alpha[\![u^1]\!]^2ds+\int_{\Gamma_\mathcal{D}^1}\alpha|u^1|^2ds+\int_\Gamma\alpha|u^1-u^2|^2ds+\|\nabla u^2\|_{0,\Omega_2}^2.$$

Proof. This follows immediately from the definition of the forms. $\square$

In our analysis we will make use of the following skew–symmetry properties:

$$\begin{aligned} \mathcal{A}(\boldsymbol{q},u^1,u^2;\boldsymbol{r},v^1,v^2) &= \mathcal{A}(-\boldsymbol{r},v^1,v^2;-\boldsymbol{q},u^1,u^2) \\ &= \mathcal{A}(\boldsymbol{r},-v^1,-v^2;\boldsymbol{q},-u^1,-u^2), \end{aligned} \tag{26}$$

for all $(\boldsymbol{q},u^1,u^2)$, $(\boldsymbol{r},v^1,v^2)$ in $\boldsymbol{Q}\times V\times W$.

2.3 Existence and uniqueness of discrete solutions

The following proposition states existence and uniqueness of approximate solutions obtained by the coupled finite element method.

Proposition 2.2 *Consider the coupled finite element method defined by equations* (16), (17) *and* (18), *and by the numerical fluxes* (19) *and* (20). *Assume that the hypothesis* (15) *on the local spaces is satisfied. If the coefficient α is strictly positive, the method defines a unique approximate solution* $(\boldsymbol{q}_h, u_h^1, u_h^2) \in \boldsymbol{M}_h \times V_h \times W_h$.

Proof. Since the discrete problem is linear and finite dimensional, it is sufficient to show that if $f = 0$, $g_{\mathcal{D}} = 0$ and $\boldsymbol{g}_{\mathcal{N}} = \boldsymbol{0}$ then $u_h^1 = u_h^2 = 0$ and $\boldsymbol{q}_h = \boldsymbol{0}$. Consider formulation (25) of the discrete problem with $\mathcal{F} = 0$. Taking $(\boldsymbol{r}, v^1, v^2) = (\boldsymbol{q}_h, u_h^1, u_h^2)$, from Proposition 2.1 we obtain $|(\boldsymbol{q}_h, u_h^1, u_h^2)|_{\mathcal{A}}^2 = 0$. This implies $\boldsymbol{q}_h = 0$ in Ω_1, $\nabla u_h^2 = 0$ in Ω_2, i.e., $u_h^2 = const$ in Ω_2, and, since $\alpha > 0$, $[\![u_h^1]\!] = 0$ on the faces in $\mathcal{E}_{\mathcal{I}}$, $u_h^1 = 0$ on $\Gamma_{\mathcal{D}}^1$, and $u_h^1 = u_h^2$ on Γ.

Assume first that the $(d-1)$–measure of $\Gamma_{\mathcal{D}}^2$ is non–zero. Since $u_h^2 = const$ in Ω_2 and $u_h^2 = 0$ on $\Gamma_{\mathcal{D}}^2$, we have $u_h^2 = 0$ in Ω_2. Consequently, since $u_h^1 = u_h^2$ on Γ, we also have $u_h^1 = 0$ on Γ. Consider now equation (21). Taking into account (24) and the fact that $[\![u_h^1]\!] = 0$ on the faces in $\mathcal{E}_{\mathcal{I}}$ and $u_h^1 = 0$ on Γ, equation (21) becomes

$$\sum_{K \in \mathcal{T}_h^1} \int_K \nabla u_h^1 \cdot \boldsymbol{r}\, d\boldsymbol{x} = 0, \qquad \forall\, \boldsymbol{r} \in \boldsymbol{M}_h \tag{27}$$

Due to (15), we have $\nabla u_h^1 = 0$ on all elements K, and, hence, $u_h^1 = const$. Since $u_h^1 = 0$ on Γ, we can conclude that $u_h^1 = 0$.

If the $(d-1)$–measure of $\Gamma_{\mathcal{D}}^2$ is zero, then the $(d-1)$–measure of $\Gamma_{\mathcal{D}}^1$ is non–zero. Again from (24), taking into account that $u_h^1 = u_h^2$ on Γ, we obtain (27), and, thus, $u_h^1 = const$. Since $u_h^1 = 0$ on $\Gamma_{\mathcal{D}}^1$, whose $(d-1)$–measure is non–zero, then $u_h^1 = 0$ in Ω_1. This implies $u_h^2 = u_h^1 = 0$ on Γ, which, together with $u_h^2 = const$ in Ω_2, gives $u_h^2 = 0$. $\square$

3 A priori error estimates

In this section we present our a priori error bounds for the coupled finite element method. We begin by stating the main result, then proceed by describing the abstract setting for its proof, following the lines of [14], and conclude by proving all the needed estimates.

3.1 The main result

First, we introduce the notation and the hypotheses needed to state Theorem 3.1 below.

We denote by $H^s(D)$, D being a domain in $\mathbb{R}^n$, $n \geq 1$, the Sobolev spaces of integer orders, and by $\|\cdot\|_{s,D}$ and $|\cdot|_{s,D}$ the usual norms and seminorms in $H^s(D)$ and $H^s(D)^d$; we omit the dependence on the domain whenever $D = \Omega$. $\mathcal{P}^\kappa(D)$ denotes the set of all polynomials of degree at most κ on D, and $\mathcal{Q}^\kappa(K)$ the polynomials of degree at most κ in each variable. For each $K \in \mathcal{T}_h^1 \cup \mathcal{T}_h^2$, we denote by h_K the diameter of K and by ρ_K the diameter of the biggest ball included in K. Recall that $h = \max_{K \in \mathcal{T}_h^1 \cup \mathcal{T}_h^2} h_K$.

Since conforming methods are very well known and we are more concerned, in our analysis of the coupled method, with the LDG part, we simply assume that the conforming finite element space W_h used for approximating the problem in the subdomain Ω_2 satisfies certain standard approximation properties. That is, we assume that for all $K \in \mathcal{T}_h^2$ the local spaces $\mathcal{S}^2(K)$ in the definition of W_h contain the image of $\mathcal{P}^m(\widehat{K})$, $m \geq 1$, through an element mapping from a reference element $\widehat{K}$ onto K, and, furthermore, that for each function $u^2 \in H^{s+2}(\Omega_2)$, $s \geq 0$, there is an element πu^2 of W_h such that

$$\begin{aligned} \|u^2 - \pi u^2\|_{1,K} &\leq C_{\text{conf}} h_K^{\min(s+1,m)} \|u^2\|_{s+2,K}, \ \forall K \in \mathcal{T}_h^2, &(28)\\ \|u^2 - \pi u^2\|_{0,\partial K} &\leq C_{\text{conf}} h_K^{\min(s+1,m)+\frac{1}{2}} \|u^2\|_{s+2,K}, \ \forall K \in \mathcal{T}_h^2. &(29) \end{aligned}$$

The constant C_{conf} depends on shape regularity conditions in $\mathcal{T}_h^2$, on the approximation order m, on d and s. Assumptions (28)–(29) allow for quite general conforming finite elements, and they are satisfied, for instance, when $\mathcal{T}_h^2$ is a regular matching grid consisting of straight triangles or tetrahedra, and $\mathcal{S}^2(K) = P^m(K)$, $\forall K \in \mathcal{T}_h^2$. In this case π can be chosen as the usual interpolant in elemental nodes. Conforming spaces with curved or iso–parametric elements and mapped polynomials (see [15]) also satisfy (28) and (29), as well as conforming spaces on meshes with certain types of hanging nodes (see [21]).

Our assumptions on the LDG side for the analysis are as follows. We assume that every element K in $\mathcal{T}_h^1$ is *affine equivalent* (see [15, Section 2.3]) to one of several reference elements in an arbitrary but fixed set; this allows for the use of elements of various shapes with possibly curved boundaries. Recall that the triangulations $\mathcal{T}_h^1$ may contain hanging nodes. We require them to be *regular*, that is, there exists a positive constant σ such that

$$\frac{h_K}{\rho_K} \leq \sigma, \qquad \forall\, K \in \mathcal{T}_h^1. \tag{30}$$

We also need to make a restriction on the ratios of the size of each element in $\mathcal{T}_h^1$ and the size of any of its neighbors. Introducing the set $\langle K, K' \rangle$ defined by

$$\langle K, K' \rangle = \begin{cases} \emptyset & \text{if } \mathrm{meas}_{(d-1)}(\partial K \cap \partial K') = 0, \\ \text{interior of } \partial K \cap \partial K' & \text{otherwise,} \end{cases}$$

this property can be stated as follows: there exists a positive constant $\delta < 1$ such that, for each element $K \in \mathcal{T}_h^1$,

$$\delta \leq \frac{h_{K'}}{h_K} \leq \delta^{-1} \qquad \forall K' : \langle K, K' \rangle \neq \emptyset \, . \tag{31}$$

We stress that K' in (31) can also be an element of $\mathcal{T}_h^2$ having one face on Γ. Assumption (31) forbids the situation where the mesh is indefinitely refined in only one of two adjacent subdomains, one of them contained in Ω_1. We point out that this is the only requirement the meshes have to satisfy at the interface Γ. Nevertheless, the above hypotheses on the meshes are not restrictive in practice, and allow for quite general triangulations.

We assume that the stabilization coefficient α in the definition (20) of the numerical fluxes is defined pointwise on the boundary of any element $K^+ \in \mathcal{T}_h^1$ as follows:

$$\alpha(\boldsymbol{x}) = \begin{cases} \vartheta \min\{h_{K^+}^{\omega}, h_{K^-}^{\omega}\} & \text{if } \boldsymbol{x} \in \langle K^+, K^- \rangle, \, K^- \in \mathcal{T}_h^1, \\ \vartheta h_{K^+}^{\omega} & \text{if } \boldsymbol{x} \in \partial K^+ \cap \Gamma_{\mathcal{D}}^1 \text{ or } \boldsymbol{x} \in \partial K^+ \cap \Gamma, \end{cases} \tag{32}$$

with $-1 \leq \omega \leq 1$ and $\vartheta > 0$. Notice that α does not need to be defined on $\partial K^+ \cap \Gamma_{\mathcal{N}}^1$. The parameter $\boldsymbol{\beta}$ is always taken such that $|\boldsymbol{\beta}|$ is of order one.

We assume that the local finite element spaces on the LDG side satisfy the following inclusions:

$$\partial_i \mathcal{S}^1(K) \subseteq \mathcal{R}(K), \quad \partial_i \mathcal{R}(K) \subseteq \mathcal{S}^1(K), \quad i = 1, \ldots, d. \tag{33}$$

Note that (33) implies (15). Furthermore, in order to guarantee approximation properties also on the LDG side, we assume that the local spaces contain at least the following polynomial spaces

$$\mathcal{P}^k(K) \subseteq \mathcal{S}^1(K), \qquad \mathcal{P}^\ell(K) \subseteq \mathcal{R}(K), \tag{34}$$

with $k \geq 1$ and $\ell \geq 0$. Since $\partial_i \mathcal{P}^k(K) \subset \mathcal{P}^{k-1}(K)$ and $\partial_i \mathcal{Q}^k(K) \subset \mathcal{Q}^k(K)$, $i = 1, \ldots, d$, conditions (33) and (34) are satisfied, for example, by

$$\mathcal{S}^1(K) = \mathcal{P}^k(K), \qquad \mathcal{R}(K) = \mathcal{P}^\ell(K), \tag{35}$$

with $k \geq 1$ and $\ell = k$ or $\ell = k-1$, or by

$$\mathcal{S}^1(K) = \mathcal{Q}^k(K), \qquad \mathcal{R}(K) = \mathcal{Q}^k(K). \tag{36}$$

We are now ready to state our main result, the proof of which is given in the next two subsections.

Theorem 3.1 *Let u be the solution of problem* (1), $(\boldsymbol{q}, u^1, u^2)$ *the corresponding solution of* (2)–(10) *and* $(\boldsymbol{q}_h, u_h^1, u_h^2)$ *the approximate solution given by the coupled finite element method* (16)–(18), *with numerical fluxes as in* (19) *and* (20). *Assume the triangulations to satisfy hypotheses* (30) *and* (31), *the local spaces in the definitions of $\boldsymbol{Q}_h$ and V_h to satisfy* (33) *and* (34), *and W_h to satisfy the approximation properties* (28)–(29). *Finally, let the stabilization parameter α be given by* (32) *with $\omega \in [-1,1]$ and $\vartheta > 0$, and $\boldsymbol{\beta}$ such that $|\boldsymbol{\beta}| = \mathcal{O}(1)$. Then, if $u \in H^{s+2}(\Omega)$ with $s \geq 0$, we have the following a priori bound for the error* $(\boldsymbol{e}^q, e^1, e^2) := (\boldsymbol{q} - \boldsymbol{q}_h, u^1 - u_h^1, u^2 - u_h^2)$:

$$|(\boldsymbol{e}^q, e^1, e^2)|_{\mathcal{A}} \leq C_1 h^{\min(s+\frac{1}{2}-\frac{\omega}{2}, k, m, l+\frac{1}{2}-\frac{\omega}{2})} \|u\|_{s+2}.$$

Furthermore, if the domain Ω is such that, for $f \in L^2(\Omega)$ and zero boundary data, u belongs to $H^2(\Omega)$ and satisfies the elliptic regularity result $\| u \|_2 \leq C_{\rm ell} \| f \|_0$, then

$$\|e^1\|_{0,\Omega_1} + \|e^2\|_{0,\Omega_2} \leq C_2 h^{\min(s+1-\omega, k+\frac{1}{2}-\frac{\omega}{2}, m+\frac{1}{2}-\frac{\omega}{2}, l+1-\omega)} \|u\|_{s+2}.$$

The constants C_i, $i = 1, 2$, are independent of the mesh–size h and depend on the constants in the approximation assumptions (28)–(29), *in the approximation results of Lemma 3.3 below, and in the inverse inequality of Lemma 3.4 below, on $|\boldsymbol{\beta}|$, on ϑ in the definition* (32) *of α, and on δ in assumption* (31); *the constant C_2 also depends on $C_{\rm ell}$.*

Let us discuss the results of Theorem 3.1.

• The exponents in the estimates of Theorem 3.1 contain the parameter ω and reach their maxima for $\omega = -1$. Consequently, the choice of α of the order $\mathcal{O}(1/h)$ yields the best convergence rates. Notice that the approximation orders k and m of u^1 and u^2, respectively, enter exactly in the same way the expressions of the convergence rates of the method.

• When $\mathcal{P}^k$– or $\mathcal{Q}^k$–elements are used for $\boldsymbol{q}$, u^1 as well as for u^2, for smooth exact solutions $u \in H^{k+2}(\Omega)$, $k \geq 1$, we obtain the error bounds

$$|(\boldsymbol{e}^q, e^1, e^2)|_{\mathcal{A}} \leq C h^k \|u\|_{k+2}, \quad \|e^1\|_{0,\Omega_1} + \|e^2\|_{0,\Omega_2} \leq C h^{k+\frac{1-\omega}{2}} \|u\|_{k+2},$$

for $\omega \in [-1,1]$. Although these rates are sharp in the sense that they are actually observed in numerical experiments (cf. Section 4 below), they are not optimal in terms of the approximation properties of the finite element spaces.

• If u^1 and u^2 are approximated by $\mathcal{P}^k$–elements and $\boldsymbol{q}$ by $\mathcal{P}^{k-1}$–elements, then *optimal* error estimates are obtained for $\omega = -1$, i.e., for $\alpha = \mathcal{O}(1/h)$. In this case, for exact solutions $u \in H^{k+1}(\Omega)$, $k \geq 1$, we have the estimates

$$|(\boldsymbol{e}^q, e^1, e^2)|_{\mathcal{A}} \leq Ch^k \|u\|_{k+1}, \qquad \|e^1\|_{0,\Omega_1} + \|e^2\|_{0,\Omega_2} \leq Ch^{k+1}\|u\|_{k+1},$$

that are optimal in terms of the approximation properties of the finite element spaces and of the regularity assumption on the exact solution.

• For $k = \ell = 0$, that is for piecewise constant approximations on the LDG side, no convergence of our method can be proved with the techniques employed in this paper. On the other hand, it has been reported in [14] that numerical experiments have shown that there is no positive order of convergence of the pure LDG method in this case. To obtain a convergent discontinuous method for piecewise constant approximations, additional stabilization parameters have to be included (see [14]).

• Sometimes it is convenient to choose mesh–dependent LDG regions in order to lower the computational cost of the method. For instance, in the application dealt with in [3], the LDG method is only used in a "small" region surrounding a slip curve where the possible hanging nodes are, and the LDG region is chosen as the union of those elements having at least one vertex on the slip curve. A fixed partition of Ω into Ω_1 and Ω_2 is assumed here only for the sake of simplicity. In fact, the convergence results of Theorem 3.1 hold true also for mesh–dependent decompositions, as can be inferred from the proof below and observed in the numerical experiments of Section 4.

3.2 The setting for the error analysis

The framework for the error analysis of the coupled formulation, a compact form of which is given by (25), is presented in this section, following the lines of [14]. We define the error $(\boldsymbol{e}^q, e^1, e^2) := (\boldsymbol{q} - \boldsymbol{q}_h, u^1 - u^1_h, u^2 - u^2_h)$, and denote by $\boldsymbol{\Pi} : \boldsymbol{Q} \to \boldsymbol{Q}_h$, $\Pi^1 : V \to V_h$ and $\Pi^2 : W \cap H^2(\Omega_2) \to W_h$ projection operators onto the finite element spaces. Since Π^2 will be chosen as a conforming finite element approximant satisfying (28)–(29), it might not be well defined on W. That is why we choose as domain of definition for Π^2 the smaller space $W \cap H^2(\Omega_2)$ whose functions are smooth enough for our purposes. We also emphasize here that $\boldsymbol{\Pi}$ and Π^1 will be taken as L^2-projections that are well defined on $\boldsymbol{Q}$ and V.

The basic ingredients of the error analysis developed in this section are two. The first one is the so–called Galerkin orthogonality property, namely,

$$\mathcal{A}(\boldsymbol{e}^q, e^1, e^2; \boldsymbol{r}, v^1, v^2) = 0 \qquad \forall (\boldsymbol{r}, v^1, v^2) \in \boldsymbol{Q}_h \times V_h \times W_h. \tag{37}$$

This property is a straightforward consequence of the consistency of the numerical fluxes.

The second ingredient is a couple of inequalities that reflect the approximation properties of the projections $\boldsymbol{\Pi}$, Π^1 and Π^2. Namely, we assume that

$$\begin{aligned} &|\mathcal{A}(\boldsymbol{q} - \boldsymbol{\Pi q}, u^1 - \Pi^1 u^1, u^2 - \Pi^2 u^2; \boldsymbol{r} - \boldsymbol{\Pi r}, v^1 - \Pi^1 v^1, v^2 - \Pi^2 v^2)| \\ &\qquad \leq C K_{\mathcal{A}}(\boldsymbol{q}, u^1, u^2; \boldsymbol{r}, v^1, v^2), \end{aligned} \tag{38}$$

for any $(\boldsymbol{q}, u^1, u^2)$, $(\boldsymbol{r}, v^1, v^2) \in \boldsymbol{Q} \times V \times [W \cap H^2(\Omega_2)]$, and

$$\begin{aligned} &|\mathcal{A}(\boldsymbol{q} - \boldsymbol{\Pi q}, \pm(u^1 - \Pi^1 u^1), \pm(u^2 - \Pi^2 u^2); \boldsymbol{r}, \pm v^1, \pm v^2)| \\ &\qquad \leq C|(\boldsymbol{r}, v^1, v^2)|_{\mathcal{A}}\, K_{\mathcal{B}}(\boldsymbol{q}, u^1, u^2), \end{aligned} \tag{39}$$

for any $(\boldsymbol{q}, u^1, u^2) \in \boldsymbol{Q} \times V \times [W \cap H^2(\Omega_2)]$ and $(\boldsymbol{r}, v^1, v^2) \in \boldsymbol{Q}_h \times V_h \times W_h$. The constants C in (38) and (39) are independent of the mesh–size. All the error estimates we are interested in can now be obtained in terms of the functionals $K_{\mathcal{A}}$ and $K_{\mathcal{B}}$. For the error in $|\cdot|_{\mathcal{A}}$ we have the following result.

Lemma 3.1 *We have*

$$|(\boldsymbol{e}^q, e^1, e^2)|_{\mathcal{A}} \leq C\big[K_{\mathcal{A}}^{1/2}(\boldsymbol{q}, u^1, u^2; \boldsymbol{q}, u^1, u^2) + K_{\mathcal{B}}(\boldsymbol{q}, u^1, u^2)\big],$$

with C independent of the mesh–size.

Proof. This is a straightforward extension of [14, Lemma 2.3]. □

The estimates for the errors $\|e^1\|_{0,\Omega_1}$ and $\|e^2\|_{0,\Omega_2}$ are based on a duality argument. Let us introduce the adjoint problem to (1):

$$\begin{aligned} -\Delta z &= \lambda &\quad& \text{in } \Omega, \\ z &= 0 && \text{on } \Gamma_{\mathcal{D}}, \\ \nabla z \cdot \boldsymbol{n} &= 0 && \text{on } \Gamma_{\mathcal{N}}, \end{aligned} \tag{40}$$

with right–hand side $\lambda \in L^2(\Omega)$. Notice that the assumptions on the domain in Theorem 3.1 guarantee that $z \in H^2(\Omega)$ and

$$\|z\|_2 \leq C_{\text{ell}} \|\lambda\|_0. \tag{41}$$

This property will be exploited later on when estimating the functionals $K_{\mathcal{A}}$ and $K_{\mathcal{B}}$. Again, problem (40) can also be written as

$$\begin{aligned} -\Delta z^i &= \lambda && \text{in } \Omega_i, \\ z^i &= 0 && \text{on } \Gamma^i_{\mathcal{D}}, \\ \nabla z^i \cdot \boldsymbol{n} &= 0 && \text{on } \Gamma^i_{\mathcal{N}}, \end{aligned} \tag{42}$$

for $i = 1, 2$, with the transmission conditions

$$z^1 = z^2 \quad \text{and} \quad \nabla z^1 \cdot \boldsymbol{n}_1 = -\nabla z^2 \cdot \boldsymbol{n}_2 \qquad \text{on } \Gamma. \tag{43}$$

Lemma 3.2 *Let z be the solution of* (40)*, (z^1, z^2) the corresponding solution of* (42)–(43)*, and $\boldsymbol{\zeta} = -\nabla z^1$. Then we have*

$$\begin{aligned} \|e^1\|_{0,\Omega_1} + \|e^2\|_{0,\Omega_2} \le C\Big(&\sup_{\lambda \in L^2(\Omega)} \frac{K_{\mathcal{A}}(\boldsymbol{q}, u^1, u^2; \boldsymbol{\zeta}, z^1, z^2)}{\|\lambda\|_0} \\ &+ K_{\mathcal{B}}(\boldsymbol{q}, u^1, u^2) \sup_{\lambda \in L^2(\Omega)} \frac{K_{\mathcal{B}}(\boldsymbol{\zeta}, z^1, z^2)}{\|\lambda\|_0}\Big), \end{aligned} \tag{44}$$

with a constant C is independent of the mesh–size.

Proof. We introduce the linear functional $\Lambda(v^1, v^2) := (\lambda, v^1)_{\Omega_1} + (\lambda, v^2)_{\Omega_2}$, $(\cdot,\cdot)_{\Omega_i}$ denoting the $L^2(\Omega_i)$–inner product, $i = 1, 2$. Then:

$$\|e_1\|_{0,\Omega_1} + \|e_2\|_{0,\Omega_2} \le C \sup_{\lambda \in L^2(\Omega)} \frac{\Lambda(e^1, e^2)}{\|\lambda\|_0}. \tag{45}$$

By definition of $\mathcal{A}$,

$$\mathcal{A}(-\boldsymbol{\zeta}, z^1, z^2; \boldsymbol{r}, v^1, v^2) = \Lambda(v^1, v^2), \tag{46}$$

for all $(\boldsymbol{r}, v^1, v^2) \in \boldsymbol{Q} \times V \times W$. Taking $(\boldsymbol{r}, v^1, v^2) = (-\boldsymbol{e}^q, e^1, e^2)$ in (46), the proof now proceeds as the one of [14, Lemma 2.4], exploiting property (26), Galerkin orthogonality (37), assumption (38) and the characterization (45) of the L^2–norm. $\square$

3.3 Proofs

In this section we prove our main results in the setting of Section 3.2. To do that, we first fix the projection operators $\boldsymbol{\Pi}$, Π^1 and Π^2. We take $\boldsymbol{\Pi}$ as the L^2-projection onto $\boldsymbol{Q}_h$, Π^1 as the L^2–projection onto V_h, and Π^2 is chosen as a conforming finite element approximant π satisfying (28) and (29). Using the techniques of [15] and recalling inclusions (34), we have the following approximation properties for $\boldsymbol{\Pi}$ and Π^1:

Lemma 3.3 *Let $K \in \mathcal{T}_h^1$ and $\boldsymbol{q} \in H^{s+1}(K)$, $s \geq 0$. Then*

$$\|\boldsymbol{q} - \boldsymbol{\Pi q}\|_{0,K} + h_K^{\frac{1}{2}} \|\boldsymbol{q} - \boldsymbol{\Pi q}\|_{0,\partial K} \leq C h_K^{\min(s,\ell)+1} \|\boldsymbol{q}\|_{s+1,K}.$$

Moreover, for $u^1 \in H^{s+2}(K)$ with $s \geq 0$, we have

$$\begin{aligned} |u^1 - \Pi^1 u^1|_{r,K} &\leq C h_K^{\min(s+1,k)+1-r} \|u^1\|_{s+2,K}, \qquad r = 0, 1, \\ \|u^1 - \Pi^1 u^1\|_{0,\partial K} &\leq C h_K^{\min(s+1,k)+\frac{1}{2}} \|u^1\|_{s+2,K}. \end{aligned}$$

The constants C solely depend on σ in inequality (30)*, on the dimension of $\mathcal{S}(K)$ and $\mathcal{R}(K)$, on d and s.*

We will also need the following standard inverse estimate:

Lemma 3.4 *There is a positive constant C_{inv} that solely depends on σ in inequality* (30)*, on the dimension of $\mathcal{R}(K)$ and on d, such that for all $\boldsymbol{s} \in \mathcal{R}(K)^d$ we have $\|\boldsymbol{s}\|_{0,\partial K} \leq C_{\text{inv}} h_K^{-1/2} \|\boldsymbol{s}\|_{0,K}$, for all $K \in \mathcal{T}_h^1$.*

In the following two subsections, estimates of $K_{\mathcal{A}}$ and $K_{\mathcal{B}}$ are given. The proof of Theorem 3.1 will then directly follow by applying the results of Corollaries 3.1 and 3.2 below to Lemmas 3.1 and 3.2.

3.3.1 The functional $K_{\mathcal{A}}$

By using Cauchy-Schwarz's inequality, the approximation properties in (28)–(29) and in Lemma 3.3, as well as the definition of α in (32), we can prove the following approximation results for the bilinear forms of our coupled method (similar arguments are used in [14, Section 3.2]).

Proposition 3.1 *Assume inclusions* (34) *to hold true, and α to be of the form* (32)*. Then, if $\boldsymbol{q} \in H^{s+1}(\Omega_1)^d$, $u^1 \in H^{s+2}(\Omega_1)$, $u^2 \in H^{s+2}(\Omega_2)$, $\boldsymbol{r} \in H^{t+1}(\Omega_1)^d$, $v^1 \in H^{t+2}(\Omega_1)$, $v^2 \in H^{t+2}(\Omega_2)$, for $s, t \geq 0$, we have the estimates*

$$\begin{aligned} &|a(\boldsymbol{q} - \boldsymbol{\Pi q}, \boldsymbol{r} - \boldsymbol{\Pi r})| \leq C h^{\min(s,\ell)+\min(t,\ell)+2} \|\boldsymbol{q}\|_{s+1,\Omega_1} \|\boldsymbol{r}\|_{t+1,\Omega_1}, \\ &|b(u^1 - \Pi^1 u^1, \boldsymbol{r} - \boldsymbol{\Pi r})| \leq C h^{\min(s+1,k)+\min(t,\ell)+1} \|u^1\|_{s+2,\Omega_1} \|\boldsymbol{r}\|_{t+1,\Omega_1}, \\ &|c(u^1 - \Pi^1 u^1, v^1 - \Pi^1 v^1)| \leq C h^{\min(s+1,k)+\min(t+1,k)+1+\omega} \|u^1\|_{s+2,\Omega_1} \|v^1\|_{t+2,\Omega_1}, \\ &|m(u^2 - \Pi^2 u^2, v^2 - \Pi^2 v^2)| \leq C h^{\min(s+1,m)+\min(t+1,m)} \|u^2\|_{s+2,\Omega_2} \|v^2\|_{t+2,\Omega_2}, \\ &|s(\boldsymbol{q} - \boldsymbol{\Pi q}, v^2 - \Pi^2 v^2)| \leq C h^{\min(s,\ell)+\min(t+1,m)+1} \|\boldsymbol{q}\|_{s+1,\Omega_1} \|v^2\|_{t+2,\Omega_2}, \\ &|t(u^1 - \Pi^1 u^1, v^2 - \Pi^2 v^2)| \leq C h^{\min(s+1,k)+\min(t+1,m)+1+\omega} \|u^1\|_{s+2,\Omega_1} \|v^2\|_{t+2,\Omega_2}, \end{aligned}$$

with C depending on the constants in the approximation assumptions (28)–(29)*, in the approximation results of Lemma 3.3, on $|\boldsymbol{\beta}|$ and on ϑ in the definition* (32) *of α, but independent of the mesh–size h.*

In the situations encountered in Lemmas 3.1 and 3.2, we obtain the following estimates for the functional $K_{\mathcal{A}}$.

Corollary 3.1 *Assume inclusions* (34) *to hold true, with $k, m \geq 1$ and $\ell \geq 0$, and the coefficient α to be of the form* (32)*, with $-1 \leq \omega \leq 1$. Assume the solution u of problem* (1) *to belong to $H^{s+2}(\Omega)$ with $s \geq 0$, and denote by $(\boldsymbol{q}, u^1, u^2)$ the corresponding solution of problem* (2)–(10)*. Then*

$$K_{\mathcal{A}}(\boldsymbol{q}, u^1, u^2; \boldsymbol{q}, u^1, u^2) \leq C_1 h^{2\min(s+1,k,m,\ell+1)} \|u\|^2_{s+2}.$$

Furthermore, let $z \in H^2(\Omega)$ be the solution of the adjoint problem (40) *with right–hand side $\lambda \in L^2(\Omega)$, and assume the elliptic regularity inequality* (41)*. Denote by (z^1, z^2) the corresponding solution of* (42)–(43) *and set $\boldsymbol{\zeta} = -\nabla z^1$. Then*

$$K_{\mathcal{A}}(\boldsymbol{q}, u^1, u^2; \boldsymbol{\zeta}, z^1, z^2) \leq C_2 h^{\min(s+1,k,m,\ell+1)+1} \|u\|_{s+2} \|\lambda\|_0.$$

The constants C_1 and C_2 depend on the same quantities as the constants C in Proposition 3.1; C_2 also depends on the elliptic regularity constant in (41).

Proof. The assertions follow immediately from Proposition 3.1, the definitions of $\mathcal{A}$ and $K_{\mathcal{A}}$, the special form of α in (32) and from the elliptic regularity estimate (41), yielding $\|\boldsymbol{\zeta}\|_{1,\Omega_1} + \|z^1\|_{2,\Omega_1} + \|z^2\|_{2,\Omega_2} \leq C\|\lambda\|_0$. $\square$

The results of Corollary 3.1 hold true for any choice of the projections $\boldsymbol{\Pi}$, Π^1 and Π^2 satisfying the approximation properties in (28)–(29) and in Lemma 3.3. The particular choice of $\boldsymbol{\Pi}$ and Π^1 as L^2-projections as well as hypothesis (31) and inclusions (33) have not been invoked so far and will be exploited in the investigation of the functional $K_{\mathcal{B}}$.

3.3.2 The functional $K_{\mathcal{B}}$

In this subsection we determine the functional $K_{\mathcal{B}}$ reflecting the approximation properties in (39). We start by noting that, after simple algebraic manipulation, we can write

$$|\mathcal{A}(\boldsymbol{q} - \boldsymbol{\Pi}\boldsymbol{q}, \pm(u^1 - \Pi^1 u^1), \pm(u^2 - \Pi^2 u^2); \boldsymbol{r}, \pm v^1, \pm v^2)| \leq T_1 + T_2 + T_3,$$

where

$$\begin{aligned}
T_1 &= \Big|\int_{\Omega_1} (\boldsymbol{q}-\boldsymbol{\Pi q})\cdot \boldsymbol{r}\,d\boldsymbol{x}\Big| + \Big|\int_{\Omega_2} \nabla(u^2-\Pi^2 u^2)\cdot \nabla v^2\,d\boldsymbol{x}\Big| \\
&\quad + \Big|\sum_{K\in\mathcal{T}_h^1}\int_K \big[(u^1-\Pi^1u^1)\nabla\cdot\boldsymbol{r} + (\boldsymbol{q}-\boldsymbol{\Pi q})\cdot\nabla v^1\big]\,d\boldsymbol{x}\Big|,\\
T_2 &= \Big|\int_{\mathcal{E}_{\mathcal{I}}} \big[\{\!\!\{u^1-\Pi^1u^1\}\!\!\} + \boldsymbol{\beta}\cdot[\![u^1-\Pi^1u^1]\!]\big][\![\boldsymbol{r}]\!]\,ds\Big| \\
&\quad + \Big|\int_{\Gamma^1_{\mathcal{N}}} (u^1-\Pi^1u^1)\boldsymbol{r}\cdot\boldsymbol{n}\,ds\Big| + \Big|\int_{\Gamma} (u^2-\Pi^2u^2)\boldsymbol{r}\cdot\boldsymbol{n}_1\,ds\Big|,\\
T_3 &= \Big|\int_{\mathcal{E}_{\mathcal{I}}} \big[\pm\{\!\!\{\boldsymbol{q}-\boldsymbol{\Pi q}\}\!\!\} \mp \boldsymbol{\beta}[\![\boldsymbol{q}-\boldsymbol{\Pi q}]\!] - \alpha[\![u^1-\Pi^1u^1]\!]\big]\cdot[\![v^1]\!]\,ds\Big| \\
&\quad + \Big|\int_{\Gamma^1_{\mathcal{D}}} \big[\pm(\boldsymbol{q}-\boldsymbol{\Pi q})\cdot\boldsymbol{n} - \alpha(u^1-\Pi^1u^1)\big]v^1\,ds\Big| \\
&\quad + \Big|\int_{\Gamma} \big[\pm(\boldsymbol{q}-\boldsymbol{\Pi q})\cdot\boldsymbol{n}_1(v^1-v^2)\,ds\Big| \\
&\quad + \Big|\int_{\Gamma} \big[\alpha\big((u^2-\Pi^2u^2)-(u^1-\Pi^1u^1)\big)\big](v^1-v^2)\,ds\Big|.
\end{aligned}$$

Estimates of the terms T_1, T_2 and T_3 are given by the following proposition.

Proposition 3.2 *Assume hypothesis* (31) *on the meshes to be satisfied, inclusions* (33) *and* (34) *to hold true, and the coefficient α to be of the form* (32)*. Then, if $\boldsymbol{q}\in H^{s+1}(\Omega_1)^d$, $u^1\in H^{s+2}(\Omega_1)$ and $u^2\in H^{s+2}(\Omega_2)$, for $s\geq 0$, and $(\boldsymbol{r},v^1,v^2)\in \boldsymbol{Q}_h\times V_h\times W_h$, the terms T_1, T_2 and T_3 above can be estimated by*

$$\begin{aligned}
T_1 &\leq C|(\boldsymbol{r},v^1,v^2)|_{\mathcal{A}}\, h^{\min(s+1,m)}\|u^2\|_{s+2,\Omega_2},\\
T_2 &\leq C|(\boldsymbol{r},v^1,v^2)|_{\mathcal{A}}\, (h^{\min(s+1,k)}\|u^1\|_{s+2,\Omega_1} + h^{\min(s+1,m)}\|u^2\|_{s+2,\Omega_2}),\\
T_3 &\leq C|(\boldsymbol{r},v^1,v^2)|_{\mathcal{A}}\, (h^{\min(s,\ell)+\frac{1}{2}-\frac{\omega}{2}}\|\boldsymbol{q}\|_{s+1,\Omega_1} \\
&\qquad + h^{\min(s+1,k)+\frac{1}{2}+\frac{\omega}{2}}\|u^1\|_{s+2,\Omega_1} + h^{\min(s+1,m)+\frac{1}{2}+\frac{\omega}{2}}\|u^2\|_{s+2,\Omega_2}),
\end{aligned}$$

with C depending on the constants in the approximation assumptions (28)–(29)*, in the approximation results of Lemma 3.3 and in the inverse inequality of Lemma 3.4, on $|\boldsymbol{\beta}|$, ϑ in the definition* (32) *of α, and on δ in assumption* (31)*, but independent of the mesh–size h.*

Proof. Since $\boldsymbol{\Pi}$ is the L^2-projection onto $\boldsymbol{Q}_h$, the first term in T_1 is zero. Furthermore, due to inclusions (33), $\int_K (u^1-\Pi^1u^1)\nabla\cdot\boldsymbol{r}\,d\boldsymbol{x} = 0$ and $\int_K(\boldsymbol{q}-$

$\boldsymbol{\Pi q}) \cdot \nabla v^1 \, d\boldsymbol{x} = 0$, and hence also the third term in T_1 is zero. Then, by Cauchy-Schwarz's inequality and the definition of the seminorm $|\cdot|_{\mathcal{A}}$, we get $T_1 \leq |(\boldsymbol{r}, v^1, v^2)|_{\mathcal{A}} \, \|\nabla(u^2 - \Pi^2 u^2)\|_{0,\Omega_2}$. The result for T_1 now follows from the approximation property (28).

For T_2, we apply Cauchy-Schwarz's inequality with weight $\sqrt{\chi}$, where $\chi(\boldsymbol{x}) = h_K$, if $\boldsymbol{x} \in \Gamma^1_{\mathcal{N}}$ or $\boldsymbol{x} \in \Gamma$, and K is the element of $\mathcal{T}^1_h$ the point $\boldsymbol{x}$ belongs to, and $\chi(\boldsymbol{x}) = \min\{h_K, h_{K'}\}$, if $\boldsymbol{x}$ belongs to a face of $\mathcal{E}_{\mathcal{I}}$, and $\boldsymbol{x} \in \langle K, K' \rangle$. In this way we obtain

$$
\begin{aligned}
T_2 \quad \leq \quad & \Big(\int_{\mathcal{E}_{\mathcal{I}}} \chi [\![\boldsymbol{r}]\!]^2 \, ds + \int_{\Gamma^1_{\mathcal{N}}} \chi |\boldsymbol{r} \cdot \boldsymbol{n}|^2 \, ds + \int_{\Gamma} \chi |\boldsymbol{r} \cdot \boldsymbol{n}_1|^2 \, ds \Big)^{\frac{1}{2}} \\
& \Big(\int_{\mathcal{E}_{\mathcal{I}}} \frac{1}{\chi} (\{\!\{u^1 - \Pi^1 u^1\}\!\} + \boldsymbol{\beta} \cdot [\![u^1 - \Pi^1 u^1]\!])^2 \, ds \\
& + \int_{\Gamma^1_{\mathcal{N}}} \frac{1}{\chi} |u^1 - \Pi^1 u^1|^2 \, ds + \int_{\Gamma} \frac{1}{\chi} |u^2 - \Pi^2 u^2|^2 \, ds \Big)^{\frac{1}{2}}.
\end{aligned}
$$

By using the inverse inequality of Lemma 3.4, the first factor can be estimated as follows:

$$
\begin{aligned}
& \int_{\mathcal{E}_{\mathcal{I}}} \chi [\![\boldsymbol{r}]\!]^2 \, ds + \int_{\Gamma^1_{\mathcal{N}}} \chi |\boldsymbol{r} \cdot \boldsymbol{n}|^2 \, ds + \int_{\Gamma} \chi |\boldsymbol{r} \cdot \boldsymbol{n}_1|^2 \, ds \\
& \leq \sum_{K \in \mathcal{T}^1_h} \sum_{e \subset \partial K} \int_e 2\, \chi \, |\, \boldsymbol{r}|_K \cdot \boldsymbol{n}_K \,|^2 \, ds \leq \sum_{K \in \mathcal{T}^1_h} 2\, \chi^{\partial K} \, \|\boldsymbol{r}|_K \cdot \boldsymbol{n}_K\|^2_{0,\partial K} \\
& \leq 2\, C_{\mathrm{inv}} \sup_{K \in \mathcal{T}^1_h} \frac{\chi^{\partial K}}{h_K} \, \|\boldsymbol{r}\|^2_0 \leq 2\, C_{\mathrm{inv}} \|\boldsymbol{r}\|^2_0 \leq 2\, C_{\mathrm{inv}} |(\boldsymbol{r}, v^1, v^2)|^2_{\mathcal{A}},
\end{aligned}
$$

where $\chi^{\partial K} = \sup\{\chi(\boldsymbol{x}) : \, \boldsymbol{x} \in \partial K\}$. Then

$$
\begin{aligned}
& T_2 \leq \sqrt{2\, C_{\mathrm{inv}}} \Big(\int_{\mathcal{E}_{\mathcal{I}}} \frac{1}{\chi} |\{\!\{u^1 - \Pi^1 u^1\}\!\} \, ds + \boldsymbol{\beta} \cdot [\![u^1 - \Pi^1 u^1]\!]|^2 \, ds \\
& + \int_{\Gamma^1_{\mathcal{N}}} \frac{1}{\chi} |u^1 - \Pi^1 u^1|^2 \, ds + \int_{\Gamma} \frac{1}{\chi} |u^2 - \Pi^2 u^2|^2 \, ds \Big)^{\frac{1}{2}} |(\boldsymbol{r}, v^1, v^2)|_{\mathcal{A}}.
\end{aligned}
$$

The result for T_2 now follows from the estimates in Lemma 3.3 and estimates (29), owing to the hypothesis (31) on the mesh.

Consider now T_3. Using Cauchy-Schwarz's inequality with weight $\sqrt{\alpha}$ for the terms involving $\boldsymbol{q} - \boldsymbol{\Pi q}$, we get

$$
\begin{aligned}
T_3 \leq |(\boldsymbol{r}, v^1, v^2)|_{\mathcal{A}} \Big(& \int_{\mathcal{E}_{\mathcal{I}}} \frac{1}{\alpha} |\{\!\{\boldsymbol{q} - \boldsymbol{\Pi q}\}\!\} - \boldsymbol{\beta} [\![\boldsymbol{q} - \boldsymbol{\Pi q}]\!]|^2 \, ds \\
& + \int_{\mathcal{E}_{\mathcal{I}}} \alpha [\![u^1 - \Pi^1 u^1]\!]^2 ds + \int_{\Gamma^1_{\mathcal{D}}} \frac{1}{\alpha} |(\boldsymbol{q} - \boldsymbol{\Pi q}) \cdot \boldsymbol{n}|^2 + \alpha |u^1 - \Pi^1 u^1|^2 ds \\
& + \int_{\Gamma} \frac{1}{\alpha} |(\boldsymbol{q} - \boldsymbol{\Pi q}) \cdot \boldsymbol{n}_1|^2 + \alpha |u^1 - \Pi^1 u^1|^2 + \alpha |u^2 - \Pi^2 u^2|^2 \, ds \Big)^{\frac{1}{2}}.
\end{aligned}
$$

Again by using the estimates in Lemma 3.3 and estimates (29), and taking into account hypothesis (31), we obtain the final estimate for T_3. $\square$

In the situations of Lemmas 3.1 and 3.2, the functional $K_{\mathcal{B}}$ can be estimated as follows.

Corollary 3.2 *Assume hypothesis* (31) *on the meshes to be satisfied, inclusions* (33) *and* (34) *to hold true with* $k, m \geq 1$ *and* $\ell \geq 0$, *and the coefficient* α *to be of the form* (32), *with* $-1 \leq \omega \leq 1$. *Assume the solution* u *of problem* (1) *to belong to* $H^{s+2}(\Omega)$ *with* $s \geq 0$, *and denote by* $(\boldsymbol{q}, u^1, u^2)$ *the solution of problem* (2)–(10). *Then*

$$
K_{\mathcal{B}}(\boldsymbol{q}, u^1, u^2) \leq C_1 h^{\min(s+\frac{1}{2}-\frac{\omega}{2}, m, k, \ell+\frac{1}{2}-\frac{\omega}{2})} \|u\|_{s+2}.
$$

Furthermore, assume the elliptic regularity inequality (41) *and let* $z \in H^2(\Omega)$ *be the solution of the adjoint problem* (40) *with right–hand side* $\lambda \in L^2(\Omega)$. *Denote by* (z^1, z^2) *the corresponding solution of* (42)–(43) *and set* $\boldsymbol{\zeta} = -\nabla z^1$. *Then*

$$
K_{\mathcal{B}}(\boldsymbol{\zeta}, z^1, z^2) \leq C_2 h^{\frac{1}{2}-\frac{\omega}{2}} \|\lambda\|_0.
$$

The constants C_1 *and* C_2 *depend on the same quantities as the constants* C *in Proposition 3.2;* C_2 *also depends on the elliptic regularity constant in* (41).

Proof. Taking into account the definition of $K_{\mathcal{B}}$ in (39), the assertions directly follow from the application of the estimates of Proposition 3.2 to the terms T_1, T_2, T_3. $\square$

The proof of Theorem 3.1 now directly follows by applying the results of Corollaries 3.1 and 3.2 to Lemmas 3.1 and 3.2.

4 Numerical results

In this section, we present a series of numerical experiments carried out on the four two–dimensional test cases described in Section 4.1. Their purpose is to validate the theoretical results proved in Section 3 in both the cases of matching and non–matching grids consisting of triangles. Numerical results in the context of the modeling of rotating electrical machines were presented in [3]. In Section 4.2, we display results for equal order approximations of the lowest order, that is $\mathcal{P}^1$–elements for u^1, u^2 and $\boldsymbol{q}$, while the performance of mixed order approximations of the lowest order, that is $\mathcal{P}^1$–elements for u^1, u^2 and piecewise constants for $\boldsymbol{q}$, is investigated in Section 4.3.

4.1 Test Cases

In all our experiments, the computational domain is chosen as the rectangle $\Omega = (-1,1) \times (-1.2, 1.2)$. We consider the following four test cases.

Test case 1: We solve the model problem (1) with homogeneous Dirichlet boundary conditions on the whole boundary $\partial\Omega$ and f chosen such that the exact solution is $u(x,y) = \cos\left(\frac{\pi}{2}x\right)\cos\left(\frac{\pi}{2.4}y\right)$. The LDG region Ω_1 is the horizontal strip $(-1,1)\times(0.3,0.3)$, and the domain Ω is meshed with matching grids. We use a sequence of four non–nested grids with decreasing mesh–sizes with a reduction factor 2. The numbers of elements of these grids are 36 (8 of which in Ω_1), 144 (32 in Ω_1), 576 (128 in Ω_1) and 2304 (512 in Ω_1). The second and third meshes are depicted in Figure 1, top.

Test case 2: We consider the same model problem as in case 1, but we mesh independently the domain Ω in the two subregions $(-1,1) \times (-1.2, 0)$ and $(-1,1) \times (0, 1.2)$, giving rise to possibly non–matching grids along the line $(-1,1) \times \{0\}$. In this case, we define the LDG region on each mesh as the union of all the elements having at least one vertex on $(-1,1) \times \{0\}$, in order to show that we obtain the predicted orders of convergence also with mesh–dependent decompositions of the domain. We use a sequence of four non–nested grids with decreasing mesh–sizes with a reduction factor 2, with hanging nodes on the line $(-1,1) \times \{0\}$. The numbers of elements are 80 (23 of which in the LDG region), 320 (47 in the LDG region), 1280 (95 in the LDG region) and 5120 (191 in the LDG region). The second and third meshes are depicted in Figure 1, bottom.

Test case 3: In order to validate the theoretical results also for inhomogeneous Dirichlet boundary conditions imposed on a part of the boundary where the LDG and the conforming region meet, we solve the model problem (1) with $f(x,y) = 3$, homogeneous Neumann boundary conditions on the

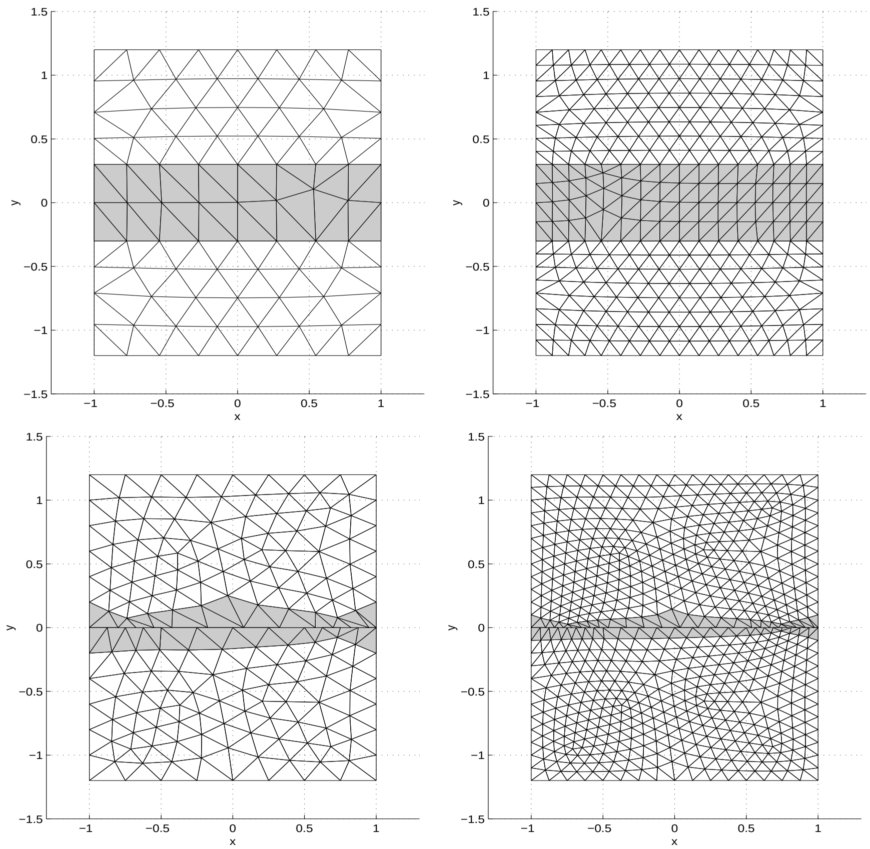

Figure 1: Grids used in the numerical experiments: non–nested grids with 144 and 576 elements with no hanging nodes (top), and with 320 and 1280 elements with hanging nodes on the line $y = 0$ (bottom). The LDG region is shadowed.

sides of the rectangle Ω with $y = \pm 1.2$, and Dirichlet boundary conditions $u(-1, y) = 0$ and $u(1, y) = 1$; the exact solution is then the quadratic function $u(x, y) = -\frac{3}{2}x^2 + \frac{1}{2}x + 2$. We use the same matching grids and LDG regions as in test case 1.

Test case 4: The last test case consists in solving the same problem as in case 3 discretized with the same sequence of non–matching grids and LDG regions as in test case 2.

4.2 Results for equal order approximations

In this subsection we present results for equal order approximations of the lowest order, i.e., all the solution components are approximated by $\mathcal{P}^1$–elements. We start by discussing the choice of the parameters α and $\boldsymbol{\beta}$.

It has been proved in [17] that the LDG method with $\mathcal{Q}^k$–elements on Cartesian grids superconverges provided that $\boldsymbol{\beta}$ is chosen in a suitable way. However, this phenomenon has not been observed, in general, on unstructured triangular meshes, and a choice of $\boldsymbol{\beta}$ that yields a better accuracy of the LDG method in the case of purely elliptic problems discretized with unstructured grids still remains to be devised. In [14], for instance, numerical experiments with unstructured grids are displayed where $\boldsymbol{\beta}$ is taken normal to the element edges and of modulus $1/2$. This choice, that can be considered as the analogon of the superconvergent flux on structured meshes, did not yield more accurate results. In our experiments, an essential difference in the results was not discovered either when varying $\boldsymbol{\beta}$ in a wide range. Thus, in the following, all the experiments are shown with $\boldsymbol{\beta} = (1, 1)$. Furthermore, the theoretical results predict a loss of half a power of h in the order of convergence for the L^2-error in u if the parameter α is chosen of order 1, whereas the optimal order is obtained with $\alpha = \mathcal{O}(1/h)$. In all the numerical tests we performed, we did not observe this loss in the rate of convergence for α constant (the same situation occurred in [14]), indicating that the results in Theorem 3.1 might be not sharp in this case. To demonstrate this phenomenon, we compare in Table 2 the errors and the reduction factors of the errors for $\alpha = 1$ and $\alpha = 1/h$ in the first test case.

stabilization parameter	reduction in h	$\mathcal{A}$–seminorm error	$\mathcal{A}$–seminorm reduction	L^2–norm of u error	L^2–norm of u reduction
$\alpha = 1$	–	6.3484e–1	–	1.2439e–1	–
	2.0	3.2093e–1	1.9781	3.0443e–2	4.0860
	2.0	1.5999e–1	2.0060	7.4957e–3	4.0613
	2.0	7.9796e–2	2.0050	1.8586e–3	4.0330
$\alpha = 1/h$	–	6.3869e–1	–	1.2545e–1	–
	2.0	3.2238e–1	1.9812	3.0750e–2	4.0795
	2.0	1.6047e–1	2.0089	7.5714e–3	4.0614
	2.0	7.9979e–2	2.0064	1.8768e–3	4.0342

Table 2: Test case 1: comparison of the choices $\alpha = 1$ and $\alpha = 1/h$. The errors and the reduction factors with respect to the previous coarser grid are reported.

	reduction in h	$\mathcal{A}$–seminorm error	reduction	L^2–norm of u error	reduction
	–	4.1970e–1	–	5.4264e–2	–
test case 2	2.0	2.2287e–1	1.8832	1.4189e–2	3.8245
	2.0	1.1428e–1	1.9501	3.6103e–3	3.9300
	2.0	5.7895e–2	1.9740	9.1301e–4	3.9543
	–	9.4501e–1	–	1.8270e–1	–
test case 3	2.0	4.5064e–1	2.0970	4.2282e–2	4.3209
	2.0	2.2324e–1	2.0186	1.0480e–2	4.0347
	2.0	1.1129e–1	2.0058	2.6111e–3	4.0135
	–	6.3781e–1	–	8.5141e–2	–
test case 4	2.0	3.3366e–1	1.9116	2.1956e–2	3.8778
	2.0	1.7076e–1	1.9539	5.6075e–3	3.9155
	2.0	8.6465e–2	1.9749	1.4216e–3	3.9445

Table 3: Errors and reduction factors for test cases 2, 3 and 4 with $\alpha = 1$.

The orders of convergence of $\mathcal{O}(h)$ for the $\mathcal{A}$–seminorm of the error and of $\mathcal{O}(h^2)$ for the L^2–norm of the error in u are clearly obtained in both cases. Note also that the actual magnitude of the errors are the same, independently of how α is chosen. Therefore, in all the following experiments with equal order approximation, we only show the results obtained for $\alpha = 1$. We also emphasize that we observed the same orders of convergence separately in the LDG and in the conforming regions, that is, $\mathcal{O}(h^2)$ for the L^2–norm of the error in u^1 and u^2, and $\mathcal{O}(h)$ for the L^2–norm of the error in $\boldsymbol{q}$ and for the H^1–seminorm of the error in u^2.

The same orders of convergence are also obtained when using the four meshes with hanging nodes with the mesh–dependent LDG region defined in test case 2. The corresponding results, together with those related to test cases 3 and 4, are reported in Table 3. Again, we point out that we observed the same orders of convergence separately in the LDG and in the conforming regions.

Finally, we want to stress the gain in terms of computational cost without loss in the approximation properties when a mesh–dependent the LDG region is chosen. To this aim, we compare the achieved accuracy for test cases 1 (fixed LDG region) and 2 (mesh–dependent LDG region) with respect to the number of non–zero entries in the coefficient matrix of the resulting algebraic linear system, after elimination of the variable $\boldsymbol{q}$ in terms of u^1 in the LDG

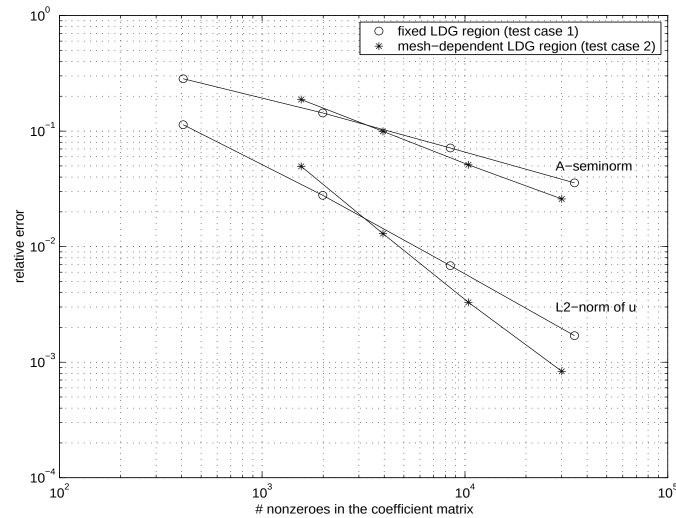

Figure 2: Test cases 1 (fixed LDG region) and 2 (mesh–dependent LDG region): comparison in terms of computational cost and achieved accuracy ($\mathcal{A}$–seminorm of the error and L^2–norm of the error in u).

elements. The size of the final algebraic system equals the number of nodes in the conforming region plus three times the number of the elements in the LDG region. For test case 1, the system sizes are 52, 178, 658 and 2530, and the numbers of the non–zero entries in the coefficient matrices are 408, 1990, 8466 and 34690, whereas for test case 2 the system sizes are 113, 309, 941 and 3165 and the non–zeroes in the matrices are 1557, 3945, 10401 and 30033. The diagram in Figure 2 shows that the same accuracy in both the $\mathcal{A}$–seminorm and the L^2–norm of u can be obtained, with a much lower computational cost for test case 2.

4.3 Results for mixed order approximations

In this subsection we display results obtained by using $\mathcal{P}^1$–elements for u^1, u^2, and piecewise constants for $\boldsymbol{q}$. As in Section 4.2 we take $\boldsymbol{\beta} = (1, 1)$, and we report in Table 4 the errors and the reduction factors of the errors for test case 1, with the choices of $\alpha = 1$ and $\alpha = 1/h$. In the following, we restrict ourselves to the choice $\alpha = 1/h$, according to the theoretical results in Theorem 3.1, and show in Table 5 the corresponding results for the test cases 2, 3 and 4. In all cases we obtain the expected convergence rates. Note, however, that for the second test case the reduction factors in the error of u are slightly better than 4, indicating that the asymptotic regime has not

stabilization parameter	reduction in h	$\mathcal{A}$–seminorm		L^2–norm of u	
		error	reduction	error	reduction
$\alpha = 1$	–	7.1111e–1	–	2.2565e–1	–
	2.0	3.6480e–1	1.9493	1.2245e–1	1.8428
	2.0	1.8374e–1	1.9854	6.2942e–2	1.9454
	2.0	9.2018e–2	1.9968	3.2590e–2	1.9313
$\alpha = 1/h$	–	7.0733e–1	–	1.3916e–1	–
	2.0	3.5965e–1	1.9667	3.7575e–2	3.7035
	2.0	1.7997e–1	1.9984	9.5550e–3	3.9325
	2.0	8.9870e–2	2.0026	2.4274e–3	3.9363

Table 4: Test case 1 with $\mathcal{P}^0$–elements for $\boldsymbol{q}$: comparison of the choices $\alpha = 1$ and $\alpha = 1/h$. The errors and the reduction factors with respect to the previous coarser grid are reported.

been reached in this case. Comparing the actual sizes of the errors with those obtained in Section 4.2 we see that the results with equal order approximations are slightly more accurate, although they are of the same order of magnitude. The orders of convergence of $\mathcal{O}(h)$ for the $\mathcal{A}$–seminorm of the error and of $\mathcal{O}(h^2)$ for the L^2–norm of the error in u are observed for $\alpha = \mathcal{O}(1/h)$, whereas $\alpha = 1$ yields a loss of one power of h in the rate of convergence of the L^2–norm of the error in u, as proved in Theorem 3.1. However, the predicted loss of half a power of h in the rate of convergence of the $\mathcal{A}$–seminorm is not be observed in this case.

Despite of the optimality of the error estimates when a lower order approximation is used for $\boldsymbol{q}$, the equal order approximation seems to be preferable from a computational point of view. We compare in Figure 3 the equal and mixed order approximations for test cases 1 (top) and 2 (bottom), in terms of achieved accuracy and number of non–zeroes in the coefficient matrix of the algebraic linear system. Note that taking this number as a measure of the computational cost does not take into account the additional cost of inverting local element matrices for the elimination of $\boldsymbol{q}$ in the equal order approximation. Since this is not relevant for small LDG regions and low order approximations, and can be simplified anyway by a suitable choice of the shape functions (see [22]), the adopted measure can be considered as fair for our purposes. The numbers of non–zeroes in the coefficient matrices are 400, 1982, 8458, 34682 (case 1) and 1545, 3933, 10389, 30021 (case 2) for the mixed order approximation, 408, 1990, 8466, 34690 (case 1) and 1557, 3945, 10401, 30033 (case 2) for the equal order approximation. Figure 3 shows that, with

	reduction in h	$\mathcal{A}$–seminorm error	$\mathcal{A}$–seminorm reduction	L^2–norm of u error	L^2–norm of u reduction
test case 2	–	4.8511e–1	–	1.1873e–1	–
	2.0	2.3794e–1	2.0388	2.4473e–2	4.8515
	2.0	1.1809e–1	2.0149	5.0973e–3	4.8012
	2.0	5.8863e–2	2.0062	1.1161e–3	4.5671
test case 3	–	1.0563	–	1.8274e–1	–
	2.0	5.1430e–1	2.0539	4.6305e–2	3.9464
	2.0	2.5566e–1	2.0117	1.2363e–2	3.7455
	2.0	1.2753e–1	2.0047	3.2121e–3	3.8489
test case 4	–	7.1595e–1	–	1.1796e–1	–
	2.0	3.5253e–1	2.0309	2.4899e–2	4.7375
	2.0	1.7553e–1	2.0084	5.8454e–3	4.2596
	2.0	8.7677e–2	2.0020	1.4389e–3	4.0424

Table 5: Test cases 2, 3 and 4 with $\mathcal{P}^0$–elements for $\boldsymbol{q}$ and $\alpha = 1/h$.

the same computational cost, the accuracy obtained with the equal order approximation, in both the $\mathcal{A}$–seminorm and in the L^2–norm of u, is slightly better than the one obtained with the mixed approach. Moreover, for a given mesh, the numbers of non–zeroes in the matrices are of the same magnitude for the two methods. Consequently, it seems not to be inefficient in practice to use the equal order approach, as also concluded in [18] for the Stokes problem.

5 Conclusions

A formulation coupling LDG and standard conforming elements for elliptic problems has been presented and analyzed, and numerical experiments validating the theoretical results have been carried out, using matching and non–matching grids. The subdomains where the different formulations are applied can be chosen arbitrarily, without affecting the order of convergence of the global method. This allows for the full exploitation of the advantages of each of the used formulations, for example, the lower computational cost of the conforming method and the ease to deal with hanging nodes of the LDG method. Despite of the optimality of the error estimates when a lower order approximation is used for $\boldsymbol{q}$, an equal order approximation for all the variables seems to be preferable. In fact, numerical experiments showed a slightly better accuracy in this case, while the computational costs remained comparable.

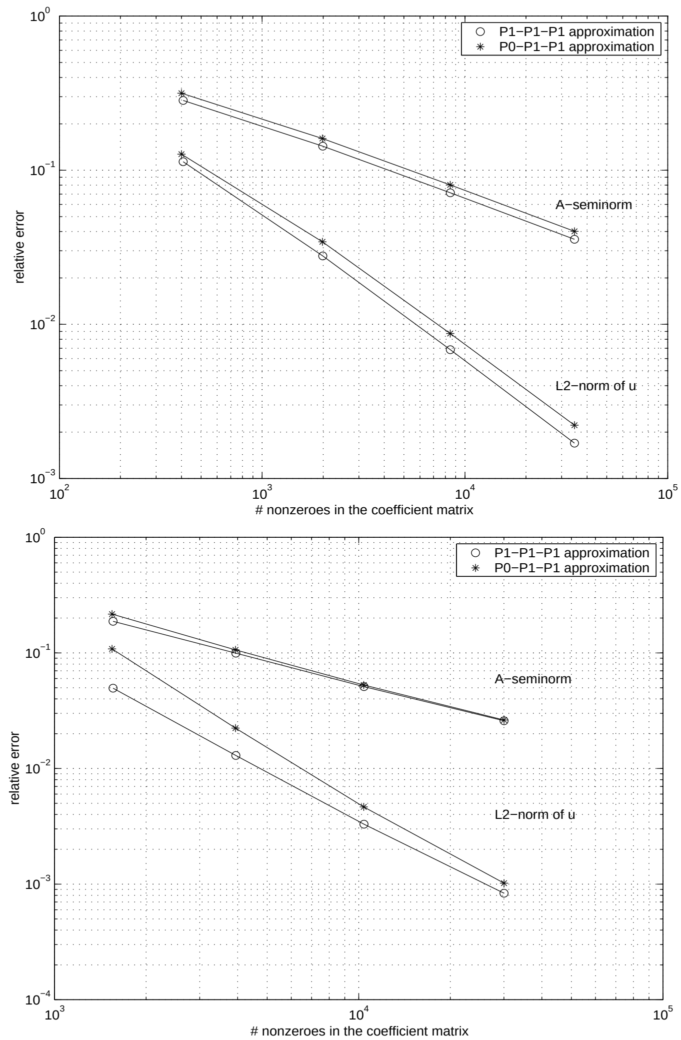

Figure 3: Test cases 1 (top) and 2 (bottom): comparison of equal order approximation with $\alpha = 1$, and mixed order approximation with $\alpha = 1/h$, in terms of computational cost and achieved accuracy ($\mathcal{A}$–seminorm of the error and L^2–norm of the error in u).

Acknowledgments

The authors want to thank Bernardo Cockburn for fruitful conversations leading to the coupling conditions for the LDG and the conforming method. They are also grateful to Piergiorgio Alotto for providing the `Fortran` code used for the numerical experiments and for helping them in its development.

References

[1] Y. Achdou, Y. Maday, and O. B. Widlund, *Iterative substructuring preconditioners for mortar element methods in two dimensions*, SIAM J. Numer. Anal. **36** (1999), 551–580.

[2] A. Agouzal, L. Lamoulie, and J. M. Thomas, *3D Domain decomposition method coupling conforming and nonconforming finite elements*, RAIRO Modél. Math. Anal. Numér. **33** (1999), 771–780.

[3] P. Alotto, A. Bertoni, I. Perugia, and D. Schötzau, *Discontinuous finite element methods for the simulation of rotating electrical machines*, Proceedings of 9th International IGTE Symposium on Numerical Field Calculation in Electrical Engineering, September 11–14, Graz, Austria, 2000.

[4] T. Arbogast, L. C. Cowsar, M. F. Wheeler, and I. Yotov, *Mixed finite element methods on nonmatching multiblock grids*, SIAM J. Numer. Anal. **37** (2000), 1295–1315.

[5] C. Baiocchi, F. Brezzi, and L. D. Marini, *Stabilization of Galerkin methods and applications to domain decomposition*, Future Tendencies in Computer Science, Control and Applied Mathematics (A. Bensoussan and J.-P. Verjus, eds.), Springer Lecture Notes in Computer Science, vol. 653, Springer, 1992, pp. 345–355.

[6] J. C. Barbosa and T. J. R. Hughes, *Boundary Lagrange multipliers in finite element methods: Error analysis in natural norms*, Numer. Math. **62** (1992), 1–15.

[7] R. Becker and P. Hansbo, *A finite element method for domain decomposition with non–matching grids*, Tech. Report 3613, INRIA Sophia Antipolis, France, 1999.

[8] F. B. Belgacem, *The mortar finite element method with Lagrange multipliers*, Numer. Math. **84** (1999), 173–197.

[9] C. Bernardi, Y. Maday, and A. T. Patera, *Domain decomposition by the mortar element method*, Asymptotic and Numerical Methods for PDEs with Critical Parameters (H.G. Kaper and M. Garbey, eds.), Kluwer, 1993, pp. 269–286.

[10] ______, *A new nonconforming approach to domain decomposition: The mortar element method*, Nonlinear Partial Differential Equations and their Applications (H. Brezis and J. Lions, eds.), Pitman, 1994, pp. 13–51.

[11] F. Brezzi and M. Fortin, *Mixed and hybrid finite element methods*, Springer-Verlag, New York, 1991.

[12] F. Brezzi, L. P. Franca, L. D. Marini, and A. Russo, *Stabilization techniques for domain decomposition methods with non-matching grids*, Domain Decomposition Methods in Sciences and Engineering (P. I. Bjørstad, M. S. Espedal, and D. E. Keyes, eds.), Domain Decomposition Press, Bergen, 1998, pp. 1–11.

[13] A. Buffa, Y. Maday, and F. Rapetti, *A sliding mesh-mortar method for a two-dimensional eddy currents model of electric engines*, Tech. Report 1141, IAN-CNR, Pavia, Italy, 1999.

[14] P. Castillo, B. Cockburn, I. Perugia, and D. Schötzau, *An a priori error analysis of the local discontinuous Galerkin method for elliptic problems*, SIAM J. Numer. Anal., to appear.

[15] P. Ciarlet, *The finite element method for elliptic problems*, North Holland, 1978.

[16] B. Cockburn, *Discontinuous Galerkin methods for convection-dominated problems*, High-Order Methods for Computational Physics (T. Barth and H. Deconink, eds.), Lect. Notes Comput. Sci. Eng., vol. 9, Springer Verlag, 1999, pp. 69–224.

[17] B. Cockburn, G. Kanschat, I. Perugia, and D. Schötzau, *Superconvergence of the local discontinuous Galerkin method for elliptic problems on Cartesian grids*, SIAM J. Numer. Anal., to appear.

[18] B. Cockburn, G. Kanschat, D. Schötzau, and C. Schwab, *Local discontinuous Galerkin methods for the Stokes system*, in preparation.

[19] B. Cockburn, G. E. Karniadakis, and C.-W. Shu (eds.), *Discontinuous Galerkin methods. Theory, computation and applications*, Lect. Notes Comput. Sci. Eng., vol. 11, Springer-Verlag, 2000.

[20] B. Cockburn and C.-W. Shu, *The local discontinuous Galerkin finite element method for convection-diffusion systems*, SIAM J. Numer. Anal. **35** (1998), 2440–2463.

[21] L. Demkowicz, J. T. Oden, W. Rachowicz, and O. Hardy, *Toward a universal hp-adaptivce FE strategy, Part I: Constrained approximation and data structure*, Comput. Methods Appl. Mech. Engrg. **77** (1989), 79–112.

[22] M. Dubiner, *Spectral methods on triangles and other domains*, J. Sci. Comp. **6** (1991), 345–390.

[23] P. Seshaiyer and M. Suri, *Uniform hp convergence results for the mortar finite element method*, Math. Comp. **69** (2000), 521–546.

[24] R. Stenberg, *On some techniques for approximating boundary conditions in the finite element method*, J. Comput. Appl. Math. **63** (1995), 139–148.

[25] ______, *Mortaring by a method of J.A. Nitsche*, Computational Mechanics. New Trends and Advances (S. Idelsohn, E. Onate, and E. Dvorkin, eds.), CIMNE Barcelona, Spain, 1998.

[26] P. Le Tallec and T. Sassi, *Domain decomposition with non-matching grids: Augmented Lagrangian approach*, Math. Comp. **64** (1995), 1367–1396.

[27] C. Wieners and B. Wohlmuth, *The coupling of mixed and conforming finite element discretizations*, Domain Decomposition Methods (J. Mandel, C. Farhat, and X.C. Cai, eds.), vol. 10, American Math. Society, 1998, pp. 453–459.